JCTC Journal of Chemical Theory and Computation

Calculation of the $\mathscr{B}$ Term of Magnetic Circular Dichroism. A Time-Dependent Density Functional Theory Approach

Michael Seth,[†] Jochen Autschbach,[‡] and Tom Ziegler*,[†]

Department of Chemistry, University of Calgary, University Drive 2500, Calgary, AB T2N-1N4, Canada, and Department of Chemistry, State University of New York at Buffalo, 312 Natural Sciences Complex, Buffalo, New York 14260-3000

Received September 12, 2006

Abstract: A method for calculating the $\mathscr{B}$ term of magnetic circular dichroism utilizing time-dependent density functional theory is presented. The expression for the $\mathscr{B}$ term is formulated through the standard sum-over-states approach, and all necessary matrix elements and transition energies are provided by the time-dependent density functional theory calculation. Test calculations of the magnetic circular dichroism spectra of ethene, propene, furan and its heavier homologues, and pyrrole and two of its derivatives are presented. The discrepancy between theory and experiment previously observed for ethene is not resolved, but the experimental spectra of the aromatic compounds are very well reproduced by the theory.

1. Introduction

Magnetic circular dichroism (MCD) spectroscopy measures the difference in absorption of left and right circularly polarized light in the presence of a magnetic field. MCD spectroscopy can provide information about the geometry and magnetic properties of the system of interest as well as new insights into the assignment of the corresponding absorption spectrum. MCD spectra are usually analyzed through three types of spectral feature, namely, the $\mathscr{A}$, $\mathscr{B}$, and $\mathscr{C}$ terms.[1,2] $\mathscr{A}$ terms occur when the degeneracy of a state involved in the transition is broken by the applied magnetic field. $\mathscr{B}$ terms arise because of the mixing between states induced by the magnetic field. $\mathscr{C}$ terms appear when the degeneracy of the ground state is broken by the magnetic field, leading to unequal populations in the ground-state components. It is generally believed that the relative importance of contributions to a MCD spectrum follows the order $\mathscr{C} > \mathscr{A} > \mathscr{B}$. Often, when $\mathscr{A}$ and/or $\mathscr{C}$ terms are present in a MCD spectrum, the influence of $\mathscr{B}$ terms is assumed to be small for the purposes of spectral interpretation.

The temperature-dependent $\mathscr{C}$ terms can be present in an MCD spectrum only if the molecule being studied has a degenerate or near-degenerate ground state. For closed-shell molecules, only $\mathscr{A}$ and $\mathscr{B}$ terms are relevant. $\mathscr{A}$ terms can arise only if a molecule has degenerate states, that is, has a 3-fold or higher rotational or improper axis in its point group. The MCD spectrum of a lower-symmetry closed-shell molecule will be made up only of $\mathscr{B}$ terms. Thus, although $\mathscr{B}$ terms are expected to be smaller in magnitude, they provide the only contribution to the MCD spectra of many molecules. Further, some experiments have found that, even for spectra dominated by $\mathscr{A}$ or $\mathscr{C}$ terms, $\mathscr{B}$ terms must be considered to fully explain what is observed.[3,4]

Recently, we have explored ways to calculate MCD $\mathscr{A}$ and $\mathscr{C}$ terms through density functional theory (DFT) calculations.[5−7] The obvious next step is to implement the calculation of $\mathscr{B}$ terms for closed-shell molecules. Our efforts in this direction are detailed in this paper. Following our previous work, we utilize DFT to describe the ground state of the system at hand and describe the excited states with time-dependent DFT (TDDFT). This choice allows us to obtain results of reasonable accuracy while retaining the ability to treat quite large molecules.

A large number of calculations of MCD $\mathscr{B}$ terms exist in the literature. Most of these calculations have utilized

* Corresponding author fax: +1-403-289-9488; e-mail: ziegler@ucalgary.ca.
[†] University of Calgary.
[‡] University of New York at Buffalo.

10.1021/ct600283t CCC: $37.00
Published on Web 12/24/2006

semiempirical methods.[8] The few ab initio calculations of MCD $\mathscr{B}$ terms include the quadratic response multiconfiguration self-consistent field study of Coriani and co-workers[9] and the generalized unrestricted Hartree−Fock sum-over states (SOS) and finite perturbation work of Honda et al.[10,11]

The outline of this paper is as follows. In the next section, we will review the equations defining the $\mathscr{B}$ term and show how TDDFT can be used in combination with these equations. The usefulness of our approach will then be illustrated through example calculations on the small molecules ethene and propene and a series of five-membered aromatic heterocyclic organic compounds.

2. Theory

Magnetic circular dichroism is defined as the difference in absorption (or absorption coefficients) of a substance with respect to left and right circularly polarized light induced by the presence of a magnetic field.

$$\Delta A_{\mathrm{MCD}}(A\rightarrow J) = \gamma(\langle|A|\mu_- |J\rangle|^2 - |\langle A|\mu_+|J\rangle|^2) \qquad (1)$$

where γ is a collection of constants, A and J are the initial and final states of a transition, and $\mu_\pm$ are the electric dipole moment operators corresponding to left and right circularly polarized light

$$\mu_- = \frac{1}{\sqrt{2}}(\mu_x - i\mu_y) \qquad (2)$$

$$\mu_+ = \frac{1}{\sqrt{2}}(\mu_x + i\mu_y) \qquad (3)$$

where i is $\sqrt{-1}$. As has already been noted, $\mathscr{B}$ terms in MCD spectroscopy arise because of the mixing between states induced by the applied magnetic field. For most magnetic fields of interest, the intensities of bands in the MCD spectrum corresponding to $\mathscr{B}$ terms vary linearly with the applied magnetic field. This MCD can be written as

$$\Delta A_{\mathrm{MCD},\mathscr{B}}(A\rightarrow J) = \gamma \mathscr{B} B f(\omega) \qquad (4)$$

where $\mathscr{B}$ is the $\mathscr{B}$ term, B is the applied magnetic field, and $f(\omega)$ is a band shape function. Throughout this work, we take $f(\omega)$ to be Gaussian in form

$$f_J(\omega) = \frac{1}{W\sqrt{\pi}} \mathrm{e}^{-(\omega-\omega_J)^2/W^2} \qquad (5)$$

for transition to state J centered at energy ω_J with width parameter W. A first-order perturbation treatment[2] gives the following expression for $\mathscr{B}$

$$\mathscr{B}(A\rightarrow J) = -\frac{2i}{3}\left[\sum_{\lambda K\kappa(K\neq A)} \frac{\langle K\kappa|\mathbf{L}|A\rangle}{\omega_K}(\langle A|\mu|J\lambda\rangle \times \langle J\lambda|\mu|K\kappa\rangle) + \sum_{\lambda K\kappa(K\neq J)} \frac{\langle J\lambda|\mathbf{L}|K\kappa\rangle}{\omega_K - \omega_J}(\langle A|\mu|J\lambda\rangle \times \langle K\kappa|\mu|A\lambda\rangle)\right] \qquad (6)$$

for nondegenerate ground state A and (possibly degenerate) excited states J and K with degenerate components λ and κ. $\mathbf{L}$ and μ are vectors composed of the Cartesian components of the angular momentum and electric dipole moment operators, respectively. ω_K is the energy of state K relative to the ground state. Equation 6 corresponds to a $\mathscr{B}$ term averaged over all possible orientations.

There is some arbitrariness with respect to sign and multiplicative constants in the definition of MCD parameters. We follow the conventions advocated by Piepho and Schatz.[2]

The first term in eq 6 describes contributions to the $\mathscr{B}$ term arising because of the magnetic-field-mediated mixing between the ground state and excited states. The second term describes contributions arising because of mixing between the excited state in the transition of interest and all other excited states.

Calculating a $\mathscr{B}$ term through eq 6 appears to be a rather formidable task. It is obviously impossible to include all excited states as required by the summation. In favorable cases, only a few states need to be included. Even if this is the case, if one wishes to make use of a wave-function-based approach to calculate $\mathscr{B}$, then one is forced to choose between methods that provide relatively low accuracy (configuration interaction singles) or those that are so prohibitively demanding in terms of computation resources [such as complete active space−self-consistent field (CASSCF) or multireference configuration interaction (MRCI)] that only relatively small molecules can be studied.

TDDFT provides a reasonable compromise between accuracy and computation expense. How can all the terms required to evaluate eq 6 be extracted from a TDDFT calculation? We consider the formulation of TDDFT utilized in the majority of implementations in quantum chemical codes, that is, that outlined by Casida.[12] The eigenvalue equation to be solved is

$$\Omega F = \omega^2 F \qquad (7)$$

where the Ω matrix is derived from the random-phase-approximation-like equations obtained from linear response TDDFT under the adiabatic approximation. The eigenvalues ω^2 are interpreted as the square of the transition energies. The eigenvectors, the "transition vector F", are closely related to the transition density from the reference state to the excited states

Most of the terms required to evaluate eq 6 can be obtained in a straightforward manner once eq 7 is solved. The ω_K terms are obviously taken directly from the eigenvalues of eq 7. Casida's original formulation included details of how to calculate $\langle A|\mu|K\rangle$ through the following formula[12]

$$\langle A|\mu|K\rangle = \sum_{ia} \sqrt{\frac{\epsilon_a - \epsilon_i}{\omega_K}}\mu_{ia}F_{ia}^K \qquad (8)$$

where ϵ_s is the energy of molecular orbital (MO) s, μ_{ia}^ξ are the matrix elements of the electric dipole moment operator with orbitals i and a, and F_{ia}^K is an element of the Kth F corresponding to the one-electron excitation from orbital i to orbital a. Here and throughout this paper, i, j, ... refer to occupied molecular orbitals; a, b, ... refer to unoccupied

orbitals; and *s*, *t*, ... refer to orbitals that could be occupied or unoccupied.

Similarly, it has been shown[13] that the terms corresponding to matrix elements of the angular momentum operator between the reference state and state *K*, $\langle A|\mathbf{L}|K\rangle$, have the form

$$\langle A|\mathbf{L}|K\rangle = \sum_{ia} \sqrt{\frac{\omega_K}{\epsilon_a - \epsilon_i}}\, \mathbf{L}_{ia} F_{ia}^K \tag{9}$$

where the slightly different form of eq 9 as compared to eq 8 arises because **L** is an antisymmetric operator while μ is a symmetric operator.

The remaining terms are matrix elements involving only excited states $\langle J|\mu|K\rangle$ and $\langle J|\mathbf{L}|K\rangle$. If $J = K$, we can use the expression given by Furche and Ahlrichs[14] utilizing the unrelaxed density to evaluate the difference between the values of a one-electron property for the reference and excited state

$$\langle J|\mathcal{O}|J\rangle - \langle A|\mathcal{O}|A\rangle = \frac{1}{2}\left[\sum_{iab} \frac{(\epsilon_a - \epsilon_i)(\epsilon_b - \epsilon_i) + \omega_J^2}{\omega_J\sqrt{(\epsilon_a - \epsilon_i)(\epsilon_b - \epsilon_i)}} F_{ia}^J F_{ib}^J \mathcal{O}_{ab} - \sum_{ija} \frac{(\epsilon_a - \epsilon_i)(\epsilon_a - \epsilon_j) + \omega_J^2}{\omega_J\sqrt{(\epsilon_a - \epsilon_i)(\epsilon_a - \epsilon_j)}} F_{ia}^J F_{ja}^J \mathcal{O}_{ij}\right] \tag{10}$$

where $\mathcal{O}_{st}$ is an element of the one-electron operator $\mathcal{O}$ over molecular orbitals *s* and *t*. $\langle A|\mathcal{O}|A\rangle$ is readily obtained from the reference state orbitals allowing $\langle J|\mathcal{O}|J\rangle$ to be calculated.

The off-diagonal elements between excited states are derived using a generalization of eq 10

$$\langle J|\mathcal{O}|K\rangle = \frac{1}{2}\left[\sum_{iab} \frac{(\epsilon_a - \epsilon_i)(\epsilon_b - \epsilon_i) + \omega_J\omega_K}{\sqrt{\omega_J\omega_K(\epsilon_a - \epsilon_i)(\epsilon_b - \epsilon_i)}} F_{ia}^J F_{ib}^K \mathcal{O}_{ab} - \sum_{ija} \frac{(\epsilon_a - \epsilon_i)(\epsilon_a - \epsilon_j) + \omega_J\omega_K}{\sqrt{\omega_J\omega_K(\epsilon_a - \epsilon_i)(\epsilon_a - \epsilon_j)}} F_{ia}^J F_{ja}^K \mathcal{O}_{ij}\right] \tag{11}$$

Equation 11 is obtained from eq 10 by relaxing the requirement that both transition densities be the same, giving $F_{ia}^J F_{ja}^K$ rather than $F_{ia}^J F_{ja}^J$ for instance. Thus, when the integrals of μ and **L** over MOs, the orbital eigenvalues, and transition energies and transition vectors available from a TDDFT calculation are inserted into eqs 8−11, all of the terms required to evaluate eq 6 are now available.

One issue remains that arises from the sum-over-states formulation of the $\mathcal{B}$ term applied here. In eq 6, the energy denominators often play an overriding role, determining the magnitude of the calculated $\mathcal{B}$ term. States that are close in energy with either the ground state or the excited state of interest generally will provide the dominant contribution to the $\mathcal{B}$ term of that transition because either ω_K or $\omega_K - \omega_J$ will be very small. This is a useful feature of the theory as it makes for simple interpretations of the observed spectra when states close in energy are present. The strong influence of the energy denominators puts very heavy demands on the theoretical method used to calculate the transition energies however. In a TDDFT calculation, the expected error of the calculated transition energies under favorable conditions (e.g., transitions well-described by one-electron excitations, a system with no transition metals) would be about 0.2 eV. Suppose two excited states (*J* and *K*) are separated by 0.15 eV. It would not be unusual if a TDDFT calculation predicted that these two states were separated by 0.05 or 0.25 eV. If the predicted energy difference was 0.05 eV, then the contribution to the $\mathcal{B}$ term of the transition $A \rightarrow J$ due to the mixing between states *K* and *J* would be too large by a factor of 3. If the predicted splitting was 0.25 eV, the $\mathcal{B}$-term contribution would be too small by a factor of 0.6. Thus, the contributions to the calculated $\mathcal{B}$ term that would be expected to be the most important are likely to be the least accurate.

It turns out that the problem caused by errors in the transition energies are less significant than they seem. From eq 6, it is apparent that, if state *K* mixes with state *J* to induce a $\mathcal{B}$ term at ω_J, then state *J* mixing with state *K* will induce a $\mathcal{B}$ term equal in magnitude but opposite in sign at energy ω_K. When two states are nearly degenerate, these two opposing $\mathcal{B}$ terms give rise to an overall band that has the derivative shaped characteristic of an $\mathcal{A}$ term.[2] It can be shown that, provided the difference in energy between the two states is significantly smaller than their absorption band widths, then the intensity of the resulting "pseudo-$\mathcal{A}$ term" is independent of that energy difference.[2] Thus, while errors in predicted transition energies may make it difficult to correctly reproduce the individual $\mathcal{B}$ terms of two closely lying states, the overall MCD spectrum is relatively insensitive to the exact energy difference, making it easier to predict the form of the spectrum.

3. Example Calculations

The approach to calculating MCD $\mathcal{B}$ terms described in the previous section was implemented into a development version of the Amsterdam Density Functional program.[15−19] In this section, we will describe several example calculations to illustrate the possibilities of the current method.

All of the calculations had several features in common. Molecular geometries were optimized in calculations utilizing valence triple-ζ basis sets with two added polarization functions (TZ2P) and the Becke-Perdew86 functional.[20−22]

Whenever the molecule of interest included the heavier elements Br, Se, or Te, relativistic effects were included by the spin-free version of the zeroth-order regularized approximation.[23−25]

It is expected that transitions to Rydberg states will be found in the energy range of interest of all of the molecules considered. A functional with correct asymptotic behavior and basis sets including diffuse functions therefore must be utilized in the TDDFT calculations. The SAOP functional[26,27] was chosen to satisfy the first requirement. For the smaller ethene and propene molecules, it was feasible to apply large, even-tempered basis sets with a double-ζ description of the core and a quadruple-ζ set describing the valence augmented with three polarization functions to all atoms. Sets of three

Table 1. Transition Energies and Oscillator Strengths of Ethene

transition	energy[a]	oscillator strength	other calculations		expt[d,e]
			MRCI[b]	STEOM-CCSD[c]	
$1^1A_g \rightarrow 1^1B_{3u}$ ($\pi \rightarrow$ 3s)	7.30	0.06	7.16	7.21 (0.08)	7.11
$1^1A_g \rightarrow 1^1B_{1g}$ ($\sigma \rightarrow \pi^*$)	7.65			8.49	
$1^1A_g \rightarrow 1^1B_{1u}$ ($\pi \rightarrow \pi^*$)	7.66	0.31	7.80	7.78 (0.37)	7.66
$1^1A_g \rightarrow 1^1B_{2g}$ ($\pi \rightarrow 3p_y$)	7.94		7.85	7.97	7.90
$1^1A_g \rightarrow 2^1B_{1g}$ ($\pi \rightarrow 3p_z$)	7.98		7.82	7.91	7.80

[a] Energies in eV. [b] Multireference configuration interaction results from ref 36. [c] Similarity transformed equation of motion coupled-cluster singles and doubles results from ref 37. Oscillator strengths in parentheses. [d] Ref 33. [e] Ref 32.

diffuse functions (3s3p3d for H and 3s3p3d3f for C) were then added to give the final QZ3P+3D basis set. For all other molecules, a similar basis set was chosen for all atoms forming part of the conjugated backbone of that molecule with the exception that only two diffuse sets (2s2p2d2f) were used to give a QZ3P+2D basis. A TZ2P basis set was taken for all nonbackbone atoms of these larger molecules. The only exception to this recipe was tellurophene as no QZ3P+2D basis set was available for tellurium. In this case, a valence quadruple-ζ basis set with four polarization functions (QZ4P) was used. This basis set is optimized for use with relativistic calculations as was that applied to Br.

The geometry optimization calculations were performed with frozen cores corresponding to [He] for O, C, and N; [Ne] for S; [Ar] for Br and Se; and [Kr] for Te. No electrons were frozen in all TDDFT calculations.

The application of basis sets with diffuse functions often leads to problems because of linear dependencies. Such issues were avoided by removing linear combinations of functions corresponding to small eigenvalues of the overlap matrix ($\leq 10^{-4}$). The overall integral accuracy parameter was chosen to be 4, which is, roughly, the number of significant digits obtained when numerically integrating the ground-state electron density.[18]

MCD spectra were simulated by placing for each transition a Gaussian band shape as given by eq 5 with bandwidth W given by

$$W = 0.1605\omega_K \tag{12}$$

where ω_K is the energy of the transition in electrovolts and is also taken as the center of the band shape. The factor of 0.1605 was chosen to give calculated bandwidths similar in size to those observed experimentally. The band shape was then multiplied by the $\mathscr{B}$ term calculated for that transition to obtain the final MCD. A comparison between any simulated spectrum and experimental results in terms of absolute intensities is difficult because estimating some contributions such as the influence of the environment on the incident light and magnetic field is challenging. To get around this problem, both the experimental and simulated spectra are scaled so that the most intense band in both spectra have the same value of ΔA at their peak.

It should be noted that the current formalism is not gauge-invariant. Previous studies have found that the results should depend very weakly on the choice of gauge.[10,11] We assume that this is the case here but will return to this point in future studies.

3.1. Ethene and Propene. The first examples that we will consider are ethene and propene. Ethene is a relatively simple molecule that was included as a test case in previous ab initio calculations of MCD spectra.[9,11] Its MCD spectrum was measured by Brith-Lindner and Allen[28] a few years ago. The MCD spectrum of propene was measured more recently.[29] Note that we follow the axis convention for ethene that puts the z axis along the C−C double bond and the x axis perpendicular to the molecular plane.

As the simplest possible molecule including a C−C double bond, the absorption spectrum of ethene has been the subject of extensive investigation both experimentally and theoretically (see, for example, refs 29−37). It is generally acknowledged that the valence ($\pi \rightarrow \pi^*$, $1^1A_g \rightarrow 1^1B_{1u}$ in D_{2h} symmetry) and Rydberg ($\pi \rightarrow$ 3s, $1^1A_g \rightarrow {}^1B_{3u}$) transitions overlap in the 6−8 eV energy range. There has been some suggestion that some of the observed bands correspond to other transitions. Evidence supporting this idea was provided by the MCD spectrum of ethene,[28] where three distinct series of peaks are observed indicating the presence of at least three states. Theoretical calculations have found that the potential-energy surface of the 1^1B_{1u} state has a saddle point at the ground-state equilibrium geometry.[31,36] It would then be expected that nonadiabatic effects could play an important part in determining the absorption spectrum of ethene, and recent calculations have supported this idea.[35,37]

The calculated transition energies and oscillator strengths of the states of ethene predicted to lie 7−8 eV above the ground state are listed in Table 1 along with some previously calculated results and experimental values. The agreement between the present vertical transition energies and high-quality MRCI and equation of motion coupled−cluster calculations[36,37] is good for the most part with all but one energy being within 0.2 eV of the other quoted values. The one exception is the $1^1A_g \rightarrow 1^1B_{1g}$ transition energy, which is rather low compared to that reported by Hazra and co-workers.[37]

The $\mathscr{B}$ terms of the $1^1A_g \rightarrow 1^1B_{3u}$ and $1^1A_g \rightarrow 1^1B_{1u}$ transitions calculated by the present method are listed in Table 2. Also listed in Table 2 are the $\mathscr{B}$ terms of the same transitions calculated by other workers.

One of the features of the SOS approach to calculating properties is that, in principle, the summation runs over all possible states. It is not always clear how many states must be included in a given treatment in order to obtain suitably converged results. Listed in Table 2 are $\mathscr{B}$ terms obtained with 25, 50, 150, or 250 states included in the expansion. For the present calculations involving ethene, these numbers

Table 2. Calculated $\mathscr{B}$ Terms of Ethene[a]

	n	$1^1A_g \rightarrow 1^1B_{3u}$	$1^1A_g \rightarrow 1^1B_{1u}$
QZ3P+3D/SAOP	250	−12.77	−6.14
QZ3P+3D/SAOP	150	−12.55	−6.49
QZ3P+3D/SAOP	50	−10.93	−4.34
QZ3P+3D/SAOP	25	−11.00	−2.46
daug-cc-pVTZ/FV-CAS [b]		−13.12	−2.04
daug-cc-pVTZ/SCF [b]		−27.21	10.55
DZ/GUHF-SECI [c]			−53.45
DZ/GUHF-SECI [c]	108		34.3

[a] $\mathscr{B}$ terms in au. *n* indicates the number of states allowed to be mixed by the magnetic field in order to evaluate $\mathscr{B}$. [b] Full-valence complete active space and Hartree−Fock results from ref 9. [c] Generalized unrestricted Hartree−Fock/single-excitation configuration interaction results from ref 11.

of states correspond to all states up to 10.9, 11.7, 14.3, and 16.36 eV, respectively. Even including only 25 states gives results that are qualitatively similar to the values calculated with 250 states. The $\mathscr{B}$ terms calculated with 25 states are both negative and are similar in magnitude to those obtained with 250 states. The $\mathscr{B}$ term of the $\pi \rightarrow \pi^*$ transition is more strongly influenced by higher-lying states, but both seem to be fairly well converged once 150 states are included.

The effort required to evaluate each individual $\mathscr{B}$ term through eq 6 increases linearly with the number of states *n*. If $\mathscr{B}$ terms for all *n* states are to be evaluated, the overall cost increases quadratically. The cost of the initial TDDFT calculation also increases with *n*. It is thus to our advantage if we can keep the number of states involved as small as possible. It is worth noting that, while *n* states may be needed to give the desired accuracy, in general, far fewer than *n* $\mathscr{B}$ terms will be of interest. If this is the case, the computational cost of the MCD calculation could be alleviated significantly by evaluating only those contributions necessary for the $\mathscr{B}$ terms of interest. The more selective algorithm would scale as *Nn* (*N* is the number of $\mathscr{B}$ terms to be calculated, usually $N \ll n$) or linearly with *n* rather than n^2. This more efficient approach has not been implemented at the present time, but it is planned for the future.

The $\mathscr{B}$ terms obtained by Coriani and co-workers using quadratic response theory and states derived from a CASSCF calculation[9] agree well with the present values. Our $\pi \rightarrow$ 3s $\mathscr{B}$ term of −12.8 au is very close to the full-valence−complete active space value of −13.1 au, while the $\mathscr{B}$ term for the $\pi \rightarrow \pi^*$ transition obtained by Coriani et al. is rather less negative than ours. The discrepancy between the present work and that of Coriani et al. may be due to the lack of dynamic correlation in the latter work. The $\mathscr{B}$ terms of the $\pi \rightarrow \pi^*$ transition calculated by Honda et al. are very different from ours. This is no doubt due to the limited basis set used in that work.

In their study of the MCD spectrum of ethene, Brith-Lindner and Allen assigned the negative bands to either the $\pi \rightarrow \pi^*$ or $\pi \rightarrow$ 3s transitions and speculated that the positive bands may be due to a $\pi \rightarrow \sigma^*$ transition.[28] Snyder and co-workers offered a different assignment suggesting that the negative bands are due to $\pi \rightarrow$ 3s and $\pi \rightarrow$ 3p transitions and positive bands are due to the $\pi \rightarrow \pi^*$ transition.[29] Our results appear to be more in line with the earlier assignments of Brith-Lindner and Allen but offer no information as to what transition may be responsible for the observed positive MCD band. Given the large nonadiabatic effects found in the absorption spectrum of ethene, it seems likely that a more detailed study including such effects will be necessary to fully understand the MCD spectrum of this species.

The current approach to calculating $\mathscr{B}$ terms offers significant scope for analysis. The TDDFT calculation can be analyzed in terms of which single-electron excitations contribute to a given transition. The SOS formulation of the $\mathscr{B}$ term naturally lends itself to analysis in terms of which states provide the major contributions to eq 6.

The TDDFT calculation of ethene gives transitions that are relatively pure. All transitions are made up at least 91% by the electron transitions given in the assignments of Table 1.

Almost all of the $\mathscr{B}$ term of the $\pi \rightarrow$ 3s ($1^1A_{1g} \rightarrow 1^1B_{3u}$) transition (−12.27 out of −12.77 au) comes from mixing of the 1^1B_{1u} with the 1^1B_{3u} state. A few other states have non-negligible contributions, but these contributions almost perfectly cancel. Given the form of eq 6, this would suggest that the $\mathscr{B}$ term of the $\pi \rightarrow \pi^*$ ($1^1A_{1g} \rightarrow 1^1B_{1u}$) transition would have a significant positive contribution of 12.27 au due to mixing of the 1^1B_{3u} state with the 1^1B_{1u} state. This is indeed the case, but this positive contribution is overtaken by large negative contributions from the 3^1B_{3u} (−11.47 au) and 1^1B_{2u} (−4.41 au) states which are predicted to be found at around 9 eV above the ground state. A few other higher-lying states also provide significant negative contributions to give the final value of about −7 au.

The absorption spectrum of propene has been studied rather less extensively than that of ethene. Under the C_s symmetry of propene, all transitions become formally allowed and rather more are observed in the 6−8 eV range than was the case for ethene. The observed spectrum in this energy range consists of a broad band with an extensive fine structure.[29,38] One of the transitions found in this band is assigned as $\pi \rightarrow \pi^*$, while the others are assigned as $\pi \rightarrow$ 3*n*, where *n* is s, p, or d.[38] The MCD spectrum of propene in the range 6−8 eV is qualitatively similar to that of ethene in that it shows negative MCD at lower energies, positive MCD at intermediate energies, and negative MCD at higher energies.[29] Snyder and co-workers assign the first negative MCD band as the $\pi \rightarrow$ 3s transition, the positive MCD band as the $\pi \rightarrow \pi^*$ transition, and more tentatively, the second negative MCD band as a $\pi \rightarrow$ 3p transition.[29]

The calculated transition energies are compared with an earlier calculation and experiment in Table 3. The agreement between our results and previous work is somewhat poorer than was the case for ethene. The $\pi \rightarrow$ 3s, the first $\pi \rightarrow$ 3p, and the $\pi \rightarrow$ 3d transitions are all within 0.2 eV of experimental results, but the $\pi \rightarrow \pi^*$ transition is calculated to be 6.81 eV, while experimentally, it is measured to be 7.2 eV; one of the $\pi \rightarrow$ 3p transitions is too high in energy, while the other is too low. The two $\sigma \rightarrow \pi^*$ transitions are probably too low, as was the case for ethene.

The calculated $\mathscr{B}$ terms for the eight transitions predicted to lie below 8.2 eV as a function of the expansion size *n* are presented in Table 4. Much like the ethene case, the

Table 3. Transition Energies and Oscillator Strengths of Propene

transition	energy[a]	oscillator strength	MRCI[b]	exptl[b]
$1^1A' \rightarrow 1A''$ ($\pi \rightarrow$ 3s)	6.58	0.008	6.89	6.55
$1^1A' \rightarrow 1A'$ ($\pi \rightarrow \pi^*$)	6.81	0.25	7.33	7.2
$1^1A' \rightarrow 1A''$ ($\pi \rightarrow$ 3p)	7.16	0.010	7.25	7.08
$1^1A' \rightarrow 1A''$ ($\pi \rightarrow$ 3p)	7.33	0.019	7.81	7.76
$1^1A' \rightarrow 1A''$ ($\sigma \rightarrow \pi^*$)	7.46	0.001		
$1^1A' \rightarrow 1A'$ ($\pi \rightarrow$ 3p)	8.01	0.016	7.77	7.6
$1^1A' \rightarrow 1A''$ ($\sigma \rightarrow \pi^*$)	8.05	0.002		
$1^1A' \rightarrow 1A''$ ($\pi \rightarrow$ 3d)	8.16	0.013	8.05	8.0

[a] Energies in eV. [b] Multireference configuration interaction calculation from ref 38.

Table 4. Calculated $\mathscr{B}$ Terms of Propene[a]

	$n = 25$	$n = 50$	$n = 150$	$n = 250$
$1^1A' \rightarrow 1A''$ ($\pi \rightarrow$ 3s)	−3.37	−2.95	−3.06	−3.12
$1^1A' \rightarrow 1A''$ ($\pi \rightarrow$ 3p)	0.59	0.65	0.00	−0.04
$1^1A' \rightarrow 1A'$ ($\pi \rightarrow \pi^*$)	−2.49	−3.90	−6.24	−5.84
$1^1A' \rightarrow 1A'$ ($\pi \rightarrow$ 3p)	−3.99	−3.94	−4.07	−4.04
$1^1A' \rightarrow 1A''$ ($\pi \rightarrow$ 3p)	−2.56	−2.45	−3.24	−3.28
$1^1A' \rightarrow 1A''$ ($\sigma \rightarrow \pi^*$)	−0.09	−0.06	0.05	0.08
$1^1A' \rightarrow 1A''$ ($\sigma \rightarrow \pi^*$)	1.35	1.18	1.19	1.18
$1^1A' \rightarrow 1A''$ ($\pi \rightarrow$ 3d)	1.87	1.62	1.80	1.80

[a] $\mathscr{B}$ terms in au. n indicates the number of states allowed to be mixed by the magnetic field in order to evaluate $\mathscr{B}$.

calculated $\mathscr{B}$ term of the $\pi \rightarrow \pi^*$ transition converges rather slowly with expansion size. The $\mathscr{B}$ terms of the other transitions are described well even by a small expansion involving 25 states. With the exception of the very small $\mathscr{B}$ terms which will contribute little to the observed MCD spectrum, the other $\mathscr{B}$ terms calculated with the 25-state expansion are within 20% of the results obtained with the 250-state expansion. Four of these five "other $\mathscr{B}$ terms" are within 10% of the $n = 250$ result when calculated with the 25-state expansion.

Also similarly to ethene, we find no sign in our calculations of the transition responsible for the positive MCD in the middle of the propene spectrum. All of the transitions expected to contribute strongly to the MCD spectrum below 8 eV have negative $\mathscr{B}$ terms. Much like ethene, it appears that nonadiabatic effects will need to be considered in order to completely explain the MCD spectrum of propene. The calculations do indicate that the MCD will become positive at higher energies however.

The interpretation of the $\mathscr{B}$ terms of the $\pi \rightarrow$ 3s and $\pi \rightarrow \pi^*$ transitions in terms of contributions to eq 6 is similar to that of ethene. The $\pi \rightarrow$ 3s ($1^1A' \rightarrow 1A''$) $\mathscr{B}$ term is dominated by the contribution from mixing the $\pi \rightarrow \pi^*$ ($1^1A' \rightarrow 1A'$) state (−2.99 au out of −3.12 au). The largest contribution to the $\mathscr{B}$ term of the $\pi \rightarrow \pi^*$ transition arises from mixing of the $\pi \rightarrow$ 3s state (2.99 au), but the overall negative $\mathscr{B}$ term is caused by several smaller negative contributions. The other four calculated $\mathscr{B}$ terms that are significant in size (>1 au) are all made up of a small number of minor contributions (≈1 au). Unlike the $\pi \rightarrow \pi^*$ transition, all of these contributions come from low energy states, meaning that these $\mathscr{B}$ terms can be calculated with a relatively small expansion, as we have seen already for ethene.

Table 5. Transition Energies and Oscillator Strengths of Furan

transition	energy[a]	oscillator strengths	CC[b]	exptl[b]
$1^1A_1 \rightarrow 1^1B_2$ ($\pi \rightarrow \pi^*$)	6.00	0.17	6.32	6.06
$1^1A_1 \rightarrow 1^1A_2$ ($\pi \rightarrow$ 3s)	6.19	0.00	6.04	5.94
$1^1A_1 \rightarrow 2^1A_1$ ($\pi \rightarrow \pi^*$)	6.33	0.0002	6.57	5.8
$1^1A_1 \rightarrow 1^1B_1$ ($\pi \rightarrow 3p_y$)	6.84	0.030	6.58	6.48
$1^1A_1 \rightarrow 2^1A_2$ ($\pi \rightarrow 3p_z$)	6.97	0.00	6.73	6.61

[a] Energies in eV [b] Coupled cluster results from ref 51.

3.2. Furan, Thiophene, Selenophene, and Tellurophene. In work published in the 1970s, Thulstrup and co-workers measured the MCD spectra of a number of five-membered-ring heterocycles including furan and pyrrole, heavier heteroatom homologues of furan, and derivatives of these molecules.[39,40] These studies provide an excellent set of data that can be used to test our implementation. In this section, we will consider furan and its homologues thiophene, selenophene, and tellurophene. In the next section, pyrrole and two derivatives of pyrrole will be discussed.

The transition energies and oscillator strengths of furan, thiophene, selenophene, and tellurophene have been calculated by Hieringer and co-workers utilizing a methodology very similar to that applied here.[41] Therefore, we shall present the transition energies and oscillator strengths from the present work as they are relevant for the calculation and analysis of MCD spectra, but there will be little discussion of these results.

As a medium-sized molecule of biological importance, absorption spectra of furan and its derivatives have been studied intensively both experimentally and theoretically (see, for example, refs 40−54). The energy range of interest for the present study is 5.0−6.5 eV. In this range, the absorption spectrum of furan is dominated by a single intense band assigned as a $\pi \rightarrow \pi^*$ transition. Some of the fine structure of this band is assigned to Rydberg transitions. Increasingly more sophisticated theoretical studies have refined these assignments and have shown that a second $\pi \rightarrow \pi^*$ transition is present in this region, although it is undetectable experimentally because of its low intensity.

The MCD spectrum of furan between 5 and 6.5 eV is dominated by a single negative band with the MCD becoming slightly positive at the highest energies.[40] As we shall see, this is in contrast to its heavier homologues.

The calculated energies and oscillator strengths of all transitions of furan up to 7.0 eV are presented in Table 5 along with coupled cluster and experimental transition energies for comparison. As has been noted previously,[41] the $\pi \rightarrow \pi^*$ transition energies calculated with the SAOP functional are a little lower than those calculated at the coupled cluster level, while the Rydberg transition energies are a little higher. The $1^1A_1 \rightarrow 1^1B_2$ ($\pi \rightarrow \pi^*$) transition has a much greater oscillator strength than the other transitions and dominates the absorption spectrum in the energy range of interest.

Table 6. Calculated $\mathscr{B}$ Terms of Furan[a]

transition	$n = 25$	$n = 50$	$n = 150$	$n = 250$
$1^1A_1 \rightarrow 1^1B_2$ ($\pi \rightarrow \pi^*$)	−9.87	−12.02	−13.54	−12.59
$1^1A_1 \rightarrow 1^1A_2$ ($\pi \rightarrow$ 3s)	0.00	0.00	0.00	0.00
$1^1A_1 \rightarrow 2^1A_1$ ($\pi \rightarrow \pi^*$)	2.81	2.74	2.74	2.72
$1^1A_1 \rightarrow 1^1B_1$ ($\pi \rightarrow 3p_y$)	3.38	3.05	3.13	2.58
$1^1A_1 \rightarrow 2^1A_2$ ($\pi \rightarrow 3p_z$)	0.00	0.00	0.00	0.00

[a] $\mathscr{B}$ terms in au. n indicates the number of states allowed to be mixed by the magnetic field in order to evaluate $\mathscr{B}$.

With the exception of the $1^1A_1 \rightarrow 2^1A_1$ ($\pi \rightarrow \pi^*$) transition, all transitions are dominated (>93%) by one single-electron excitation from a π orbital to the appropriate π or Rydberg orbital. The $1^1A_1 \rightarrow 2^1A_1$ ($\pi \rightarrow \pi^*$) transition is approximately a 50/50 mix of the two $\pi \rightarrow \pi^*$ orbital excitations with A_1 symmetry.[41]

The calculated MCD $\mathscr{B}$ terms of the five lowest transitions of furan are listed in Table 6, and the simulated MCD spectrum of furan obtained from the $n = 250$ parameters is compared with the experimental spectrum in Figure 1a.

The most obvious conclusion that can be drawn from Figure 1a is that the simulated spectrum reproduces all of the important features of the observed spectrum. Both have a large negative band and slightly positive MCD at higher energies. From Table 6, it is apparent that the negative MCD is due to the significant $\mathscr{B}$ term of the $1^1A_1 \rightarrow 1^1B_2$ ($\pi \rightarrow \pi^*$) transition. The negative MCD of this transition overwhelms the lesser positive MCD at a little higher energy from the other $\pi \rightarrow \pi^*$ transition. The positive $\mathscr{B}$ term of the $1^1A_1 \rightarrow 1^1B_1$ transition is far enough away from the $1^1A_1 \rightarrow 1^1B_2$ one to be able to produce some positive MCD at the higher-energy end of the spectrum.

One difference between the calculated and simulated spectra is the energy of minimum MCD. Experimentally, it is at about 5.8 eV, while it is calculated to be just below 6 eV. This is a little surprising given the close agreement between the calculated transition energy and that observed experimentally (Table 5). The greater error in the location of the MCD band suggests that the weaker positive bands in this region, which have a non-negligible influence on the overall spectrum, are a little too low in energy in the calculation.

Table 6 lists $\mathscr{B}$ terms calculated with differing numbers of states included in the expansion given by eq 6. Much like ethene and propene, it is apparent that the MCD spectrum of furan between 5 and 7 eV can be described qualitatively by a small 25-state expansion. Of the three nonzero $\mathscr{B}$ terms, only that of the $1^1A_1 \rightarrow 1^1B_2$ transition changes by more than 1 au when going from a 25-state expansion to a 250-state expansion. A 50-state expansion reproduces the results of the 250-state expansion closely. A total of 50 states represent all states calculated to lie below 10.42 eV, while the 250 states lie below 14.87 eV.

The slower convergence of the $\mathscr{B}$ term of the $1^1A_1 \rightarrow 1^1B_2$ transition with respect to the number of states included in eq 6 indicates that a number of states make significant contributions to the perturbation expansion of this $\mathscr{B}$ term. This is indeed the case. Three states, 2^1A_1, 3^1A_1, and 10^1B_2, contribute over 1.0 au through mixing with the 1^1B_2 state with −3.3, −2.4, and −1.9 au, respectively. Although it is close in energy to the 1^1B_2 state, the 1^1B_1 state only contributes 0.4 au because the magnetic field only induces weak mixing between the two states ($\langle 1^1B_2|L_z|1^1B_1\rangle$ is −0.04 au).

Turning now to thiophene, selenophene, and tellurophene, the absorption spectra of the first two molecules are much like that of furan with a single broad band between 4.5 and 6.5 eV. The spectrum of tellurophene exhibits more structure with an intense peak at around 4.5 eV and weaker peaks near 5.0 and 6.0 eV.[40] The MCD spectra of thiophene and selenophene are similar to each other but different from that of furan. These spectra show positive MCD at lower energies and negative MCD at higher energies, giving an overall derivative shaped band characteristic of an MCD $\mathscr{A}$ term or two near-degenerate $\mathscr{B}$ terms of opposite sign.[40] These MCD spectra provided good evidence that there are at least two states that contribute to the observed absorption band. The MCD spectrum of tellurophene is more similar to that of furan as it is dominated by a single negative band. It differs from the furan spectrum, however, in that it has a weak positive band at lower energies than the negative band and at higher energies the MCD becomes more negative again.

Calculated transition energies and oscillator strengths of thiophene, selenophene, and tellurophene up to 7.0 eV are listed in Table 7. The $\pi \rightarrow \pi^*$ transitions decrease in energy from furan to tellurophene. The $1^1A_1 \rightarrow 2^1A_1$ transition decreases more rapidly so that, while for furan the $1^1A_1 \rightarrow 1^1B_2$ transition is lower in energy than the $1^1A_1 \rightarrow 2^1A_1$ transition, for thiophene the two transitions are nearly degenerate and for tellurophene the $1^1A_1 \rightarrow 2^1A_1$ transition is far enough below the $1^1A_1 \rightarrow 1^1B_2$ transition that the two bands can be resolved.[40] The $1^1A_1 \rightarrow 2^1A_1$ transition gains in intensity, and the $1^1A_1 \rightarrow 1^1B_2$ transition decreases in intensity from furan to tellurophene. The Rydberg states decrease in energy and increase in intensity as the heteroatom becomes heavier. The assignments of the $\pi \rightarrow \pi^*$ transitions excitation are clear-cut; in all cases, one MO to MO excitation dominates (>80%) the transition density. Some of the higher-lying Rydberg transition have more mixed character, but the excitation with the greatest contribution is used in the assignments.

The calculated MCD $\mathscr{B}$ terms of all transitions up to 7.0 eV can be found in Table 8, and the simulated MCD spectra of thiophene, selenophene, and tellurophene obtained from these terms are presented in Figure 1b−d. As was noted earlier, the MCD spectra of thiophene and selenophene imply the presence of overlapping oppositely signed $\mathscr{B}$ terms from two nearly degenerate states. Our calculations support this conclusion. We find that the two lowest $\pi \rightarrow \pi^*$ (2^1A_1 and 1^1B_2) states of thiophene and selenophene interact strongly in the presence of a magnetic field to give the large $\mathscr{B}$ terms listed in Table 8. The $\pi \rightarrow \pi^*$ states are close enough in energy to produce pseudo-$\mathscr{A}$ terms (Figure 1b,c). The $\mathscr{B}$ terms of the other states listed in Table 8 have little impact on the overall MCD spectrum.

Not surprisingly, the $\mathscr{B}$ terms of the 2^1A_1 and 1^1B_2 states of thiophene and selenophene are almost completely due to the interaction between these two states (±320 au for

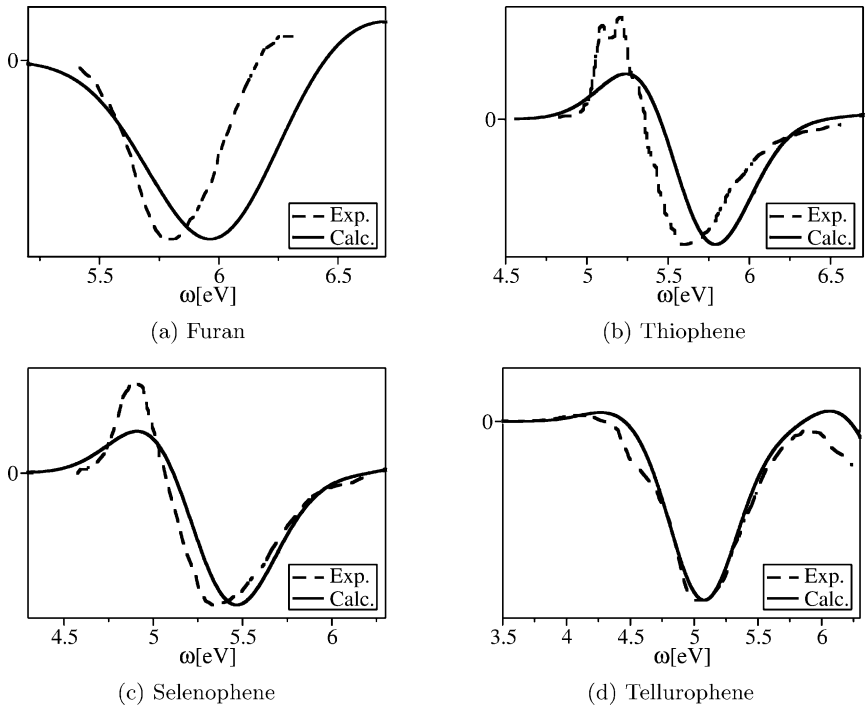

Figure 1. Experimental and simulated MCD spectra of furan, thiophene, selenophene, and tellurophene.

Table 7. Transition Energies and Oscillator Strengths of Thiophene, Selenophene, and Tellurophene

	thiophene		selenophene		tellurophene	
transition	energy[a]	oscillator strengths	energy[a]	oscillator strengths	energy[a]	oscillator strengths
$1^1A_1 \rightarrow 2^1A_1$ ($\pi \rightarrow \pi^*$)	5.56	0.062	5.14	0.088	4.42	0.100
$1^1A_1 \rightarrow 1^1B_2$ ($\pi \rightarrow \pi^*$)	5.60	0.070	5.36	0.059	5.06	0.032
$1^1A_1 \rightarrow 1^1B_1$ ($\pi \rightarrow p_y$)	5.73	0.0035	5.21	0.0022	4.41	0.015
$1^1A_1 \rightarrow 1^1A_2$ ($\pi \rightarrow p_y$)	6.03	0.00	5.28	0.00	4.06	0.00
$1^1A_1 \rightarrow 2^1A_2$ ($\pi \rightarrow s$)	6.22	0.00	6.22	0.00	5.90	0.00
$1^1A_1 \rightarrow 2^1B_1$ ($\pi \rightarrow s$)	6.53	3.69×10^{-7}	6.27	0.0033	5.50	0.0065
$1^1A_1 \rightarrow 3^1A_2$ ($\pi \rightarrow p_z$)	6.98	0.00	6.49	0.00	6.63	0.00
$1^1A_1 \rightarrow 3^1B_1$ ($\sigma \rightarrow \pi^*$)			6.59	0.0065	5.92	5.96×10^{-5}
$1^1A_1 \rightarrow 4^1B_1$ ($\pi \rightarrow p_z$)			6.68	0.0053	6.26	0.087
$1^1A_1 \rightarrow 2^1B_2$ ($\pi \rightarrow \pi^*$)			6.82	0.065	6.08	0.0069
$1^1A_1 \rightarrow 3^1A_1$ ($\pi \rightarrow \pi^*$)			6.90	0.11	6.58	0.026
$1^1A_1 \rightarrow 4^1A_2$ ($\pi \rightarrow d$)					5.99	0.00
$1^1A_1 \rightarrow 6^1A_2$ ($\pi \rightarrow p_z$)					6.24	0.00
$1^1A_1 \rightarrow 5^1B_1$ ($\pi \rightarrow d$)					5.71	0.0031
$1^1A_1 \rightarrow 5^1A_2$ ($\sigma \rightarrow \pi^*$)					6.40	0.00
$1^1A_1 \rightarrow 6^1B_1$ ($\pi \rightarrow p_y$)					6.65	0.019
$1^1A_1 \rightarrow 7^1B_1$ ($\pi \rightarrow d$)					6.71	0.026
$1^1A_1 \rightarrow 4^1A_1$ ($\pi \rightarrow p_x$)					6.77	0.040
$1^1A_1 \rightarrow 3^1B_2$ ($\sigma \rightarrow p_y$)					6.78	0.25

[a] Energies in eV.

thiophene and ±59 au for selenophene). The two $\mathscr{B}$ terms are not exactly equal in magnitude. Mixing between the higher-energy $\pi \rightarrow \pi^*$ states and the 2^1A_1 and 1^1B_2 states adds non-negligible negative contributions to the $\mathscr{B}$ terms of both the lower-energy $\pi \rightarrow \pi^*$ states. This results in $\mathscr{B}$ terms of the 1^1B_2 states that are larger in magnitude than those of the 2^1A_1 states and gives the slightly asymmetric form of the pseudo-$\mathscr{A}$ terms.

Although it is also close in energy to the 2^1A_1 and 1^1B_2 states, the 1^1B_1 state has a much smaller $\mathscr{B}$ term. The weaker MCD caused by this state is due to the lower intensity of the transition (smaller $\langle A|\mu|J\rangle$ term in eq 6) and weaker mixing between states induced by the magnetic field (smaller $\langle J|\mathbf{L}|K\rangle$ term in eq 6).

The situation is rather different in tellurophene. Here, the two lowest-energy $\pi \rightarrow \pi^*$ states are split in energy by more than 0.6 eV, but the lowest Rydberg state (1^1B_1) is very close in energy to the lowest $\pi \rightarrow \pi^*$ state (2^1A_1). Although they are almost degenerate, these two states induce only moderate $\mathscr{B}$ terms because the interaction as measured by $\langle J|\mathbf{L}|K\rangle$ is still small. The 2^1A_1 and 1^1B_2 states still interact strongly to produce the significant negative $\mathscr{B}$ term of the 1^1B_2 state.

Table 8. Calculated $\mathscr{B}$ Terms of Thiophene, Selenophene, and Tellurophene[a]

	thiophene		selenophene		tellurophene	
transition	$n = 50$	$n = 250$	$n = 50$	$n = 250$	$n = 50$	$n = 250$
$1^1A_1 \rightarrow 2^1A_1$ ($\pi \rightarrow \pi^*$)	309.80	309.08	47.25	45.24	−10.42	−11.62
$1^1A_1 \rightarrow 1^1B_2$ ($\pi \rightarrow \pi^*$)	−336.71	−338.70	−66.17	−68.15	−22.36	−23.54
$1^1A_1 \rightarrow 1^1B_1$ ($\pi \rightarrow p_y$)	6.16	6.07	−2.85	−3.09	13.08	12.94
$1^1A_1 \rightarrow 1^1A_2$ ($\pi \rightarrow p_y$)	0.00	0.00	0.00	0.00	0.00	0.00
$1^1A_1 \rightarrow 2^1A_2$ ($\pi \rightarrow s$)	0.00	0.00	0.00	0.00	0.00	0.00
$1^1A_1 \rightarrow 2^1B_1$ ($\pi \rightarrow s$)	−0.008	−0.008	−1.14	−1.04	−2.15	−1.90
$1^1A_1 \rightarrow 3^1A_2$ ($\pi \rightarrow p_z$)	0.00	0.0	0.00	0.00	0.00	0.00
$1^1A_1 \rightarrow 3^1B_1$ ($\sigma \rightarrow \pi^*$)			1.14	1.37	−0.28	−0.17
$1^1A_1 \rightarrow 4^1B_1$ ($\pi \rightarrow p_z$)			0.52	−0.13	0.24	0.18
$1^1A_1 \rightarrow 2^1B_2$ ($\pi \rightarrow \pi^*$)			20.66	18.68	−1.51	−1.40
$1^1A_1 \rightarrow 3^1A_1$ ($\pi \rightarrow \pi^*$)			−15.26	−22.10	−10.89	−13.65
$1^1A_1 \rightarrow 4^1A_2$ ($\pi \rightarrow d$)					0.00	0.00
$1^1A_1 \rightarrow 6^1A_2$ ($\pi \rightarrow p_z$)					6.40	6.79
$1^1A_1 \rightarrow 5^1B_1$ ($\pi \rightarrow d$)					0.00	0.00
$1^1A_1 \rightarrow 5^1A_2$ ($\sigma \rightarrow \pi^*$)					0.00	0.00
$1^1A_1 \rightarrow 6^1B_1$ ($\pi \rightarrow p_y$)					18.29	17.32
$1^1A_1 \rightarrow 7^1B_1$ ($\pi \rightarrow d$)					−25.98	−25.02
$1^1A_1 \rightarrow 4^1A_1$ ($\pi \rightarrow p_x$)					500.18	504.66
$1^1A_1 \rightarrow 3^1B_2$ ($\sigma \rightarrow p_y$)					−495.12	−503.34

[a] Energies in eV.

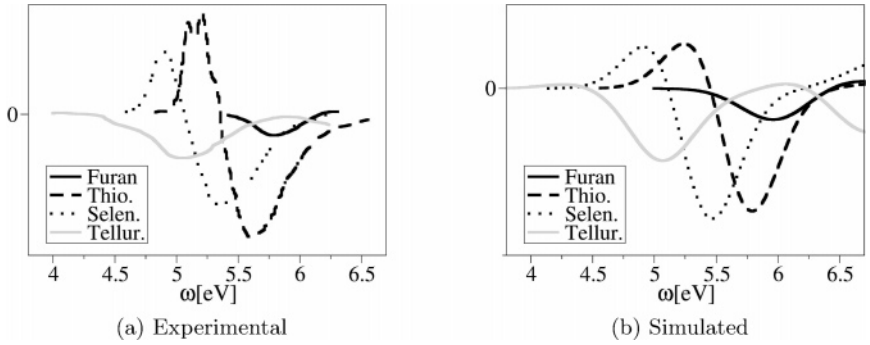

Figure 2. Experimental and simulated MCD spectra of furan, thiophene, selenophene, and tellurophene.

The higher $\pi \rightarrow \pi^*$ states again make non-negligible negative contributions to the $\mathscr{B}$ terms of the 2^1A_1 and 1^1B_2 states.

The negative MCD from the $\mathscr{B}$ terms of the 2^1A_1 and 1^1B_2 states of tellurophene nearly but not completely cancel that from the positive $\mathscr{B}$ term of the 1^1B_1 state, giving the small positive shoulder at low energies in the MCD spectrum of tellurophene (Figure 1d). At higher energies, the MCD of the two $\pi \rightarrow \pi^*$ transitions reinforce each other and a strong negative band in the MCD spectrum is observed. The trend toward negative MCD at higher energies is due to the significant negative $\mathscr{B}$ term of the second $\pi \rightarrow \pi^*$ state with A_1 symmetry that is predicted to be found just beyond the energy range of the experimental MCD spectrum.

The simulated MCD spectra of thiophene, selenophene, and tellurophene utilized $\mathscr{B}$-term calculations including 250 states in the perturbation expansions. Also listed in Table 8 are the results of calculations utilizing only the lowest 50 states. As was the case with furan, it appears that the much smaller 50-state calculations give similar results to the large 250-state calculations.

The discussion so far has focused on how well the calculations reproduce trends within a spectrum. The MCD sign, band shapes, and band maxima locations of simulated spectra have been compared with the corresponding experimental spectrum. What has been considered in much less detail is whether trends across the spectra and in particular the intensity of one spectrum as compared with another. We will discuss this issue now. The experimental MCD spectra of furan, thiophene, selenophene, and tellurophene are collected in one place in Figure 2a. The spectra are all similar in intensity in the sense that all of the major band maxima fall within 1 order of magnitude. If the greatest MCD (negative or positive) of the furan spectrum is taken as 1, the greatest MCD of the spectra follows the approximate ratio 1:5.7:4.3:2.0 for furan/thiophene/selenophene/tellurophene. The equivalent comparison of the simulated spectra can be found in Figure 2b. The data in this figure have of course not been rescaled and are derived directly from the calculated $\mathscr{B}$ terms. Figure 2a and b are remarkably similar. The only major discrepancy is that the simulated thiophene spectrum is somewhat too low in intensity as compared to the other three. The simulated spectra have a furan/thiophene/selenophene/tellurophene ratio of 1:3.9:4.1:2.3. These results suggest that not only can the features of individual MCD spectra be reproduced but so can the relationships between spectra of similar compounds.

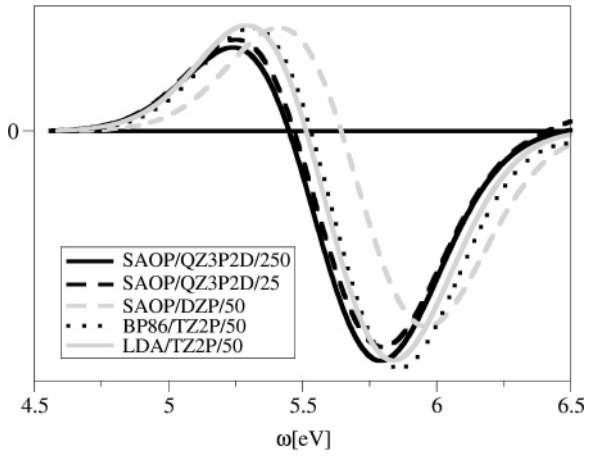

Figure 3. Simulated MCD spectra of thiophene with different functionals and basis sets. "250", "50", or "25" refers to the number of states used in the $\mathscr{B}$-term expansion.

The MCD spectra of thiophene and selenophene are examples of spectra that are ideally suited to be calculated with the approach described here. Two states have large, oppositely signed $\mathscr{B}$ terms that are produced by the mixing of a small number of low-energy states. It would therefore be expected that a TDDFT calculation involving only relatively small numbers of transitions would be required to give a reasonable simulation of the spectrum and to aid in the interpretation of the experimental spectra. In the case of thiophene and selenophene, the situation is further simplified because the two important excited states both arise because of valence excitations. Therefore, it should be possible to describe transitions to these states with TDDFT calculations involving standard generalized gradient approximations and simple basis sets rather than asymptotically corrected functionals and extensive basis sets that must include diffuse functions. To illustrate this point, we present the MCD spectrum of thiophene obtained using parameters derived from calculations with smaller numbers of states included in the expansion of eq 6, with smaller basis sets and with nonasymptotically corrected functionals (Figure 3). In this figure, BP86 is the combination of Becke's 1988 correlation functional and Perdew's 1986 exchange functional,[20−22] LDA indicates the use of the simple local density approximation, and DZP indicates a valence double-ζ basis set with a single set of polarization functions on each atom. All the spectra in Figure 3 are very similar to each other. The agreement is especially remarkable given the range of values obtained in these calculations for the $\mathscr{B}$ terms of the important two $\pi \rightarrow \pi^*$ transitions. For instance, the $\mathscr{B}$ terms obtained in the SAOP/QZ3P2D/250 calculation are on the order of $\pm$300 au, while those obtained from the SAOP/DZP/50 calculation are on the order of $\pm$100 au. The results were not rescaled, so all calculations produce a simulated MCD spectrum with very similar intensities as well as shape.

3.3. Pyrrole, *N*-Methylpyrrole, and 2,5-Dimethylpyrrole. Thulstrup and co-workers have also examined the MCD spectra of pyrrole and several of its derivatives including *N*-methylpyrrole, 1,2-dimethylpyrrole, 2,4-dimethylpyrrole, 2,5-dimethylpyrrole, and 1,2,5-trimethylpyrrole.[40] The absorption spectra of these six compounds in the range 5−6.5 eV are all very similar to each other and consist of a broad peak at around 6 eV and increasing absorption intensity at higher energies.[40]

In contrast, the MCD spectra of pyrrole and its derivatives show considerable variation. The spectrum of pyrrole between 5.5 and 6.5 eV shows only negative MCD and one peak. The MCD spectra of 1,2-dimethylpyrrole, 2,4-dimethylpyrrole, and 2,5-dimethylpyrrole have negative MCD at low energies, positive MCD at around 6 eV, and then negative MCD again at higher energies. Finally, the MCD spectra of *N*-methylpyrrole and 1,2,5-trimethylpyrrole include a positive MCD peak below 6 eV and negative MCD at higher energies.

In this section, we present calculations of the MCD spectra of pyrrole, *N*-methylpyrrole, and 2,5-dimethylpyrrole, molecules that cover the three types of MCD spectra mentioned above. The calculated transition energies and oscillator strengths of all three molecules are listed in Table 9.

As might be expected, the results for pyrrole in Table 9 share many features with the previous furan calculations. Two $\pi \rightarrow \pi^*$ transitions appear in the region of interest: the $1^1A_1 \rightarrow 1^1B_2$ transition, which is predicted to have a large oscillator strength, and the $1^1A_1 \rightarrow 2^1A_1$ transition, which is predicted to be very weak in intensity. These two states are calculated to be nearly degenerate, which will certainly have consequences for the predicted MCD spectrum of pyrrole. A number of Rydberg transitions of low intensity are also predicted to lie between 5 and 6.5 eV.

There is considerable disagreement among theoretical calculations dealing with the band in the absorption spectrum of pyrrole centered at 6 eV.[41,48,52,55−58] It is generally agreed that the lowest-energy peaks in this band are due to the $1^1A_1 \rightarrow 1^1A_2$ transition with a vertical excitation energy similar to that obtained in the present work. The most sophisticated and recent studies also agree for the most part on the location and assignment of most of the other Rydberg transitions. There is still disagreement with respect to the $\pi \rightarrow \pi^*$ transitions. In particular, there is disagreement as to the ordering of these two states, their energies, and whether they are pure $\pi \rightarrow \pi^*$ in character or whether some mixing of Rydberg character occurs. A detailed discussion of the controversy is beyond the scope of this work, but it appears that our results are most in line with the most recent CASPT2 studies of Roos and co-workers.[56] The CASPT2 transition energies from ref 56 are somewhat lower than those given here, but this study predicted that the vertical transition energies to the 1^1B_2 and 2^1A_1 states would be very similar, that the $1^1A_1 \rightarrow 1^1B_2$ transition would have a much higher oscillator strength than the other nearby transitions, and that there would be little $\pi \rightarrow \pi^*$ and Rydberg mixing. Similar conclusions could be drawn from the results of Table 9. The order of the 1^1B_2 and 2^1A_1 states given by Roos and co-workers is the reverse of that presented here, but these two states are nearly degenerate, and their ordering will be very difficult to pin down with confidence.

The transition energies and oscillator strengths calculated for *N*-methylpyrrole and 2,5-dimethylpyrrole follow a similar pattern to those of pyrrole. One of the lower-energy $\pi \rightarrow \pi^*$ transitions has a much greater intensity than all of the

Table 9. Transition Energies, Oscillator Strengths, and $\mathscr{B}$ Terms of Pyrrole, *N*-Methylpyrrole, and 2,5-Dimethylpyrrole[a]

transition	energy[a]	oscillator strengths	*B*	
			$n = 50$	$n = 250$
Pyrrole				
$1^1A_1 \rightarrow 1^1A_2$ ($\pi \rightarrow$ 3s)	5.26	0.00	0.00	0.00
$1^1A_1 \rightarrow 1^1B_1$ ($\pi \rightarrow$ 3s)	6.10	7.16×10^{-6}	0.011	0.022
$1^1A_1 \rightarrow 1^1B_2$ ($\pi \rightarrow \pi^*$)	6.20	0.19	89.49	89.01
$1^1A_1 \rightarrow 1^1A_1$ ($\pi \rightarrow \pi^*$)	6.21	1.21×10^{-4}	−91.17	−91.18
$1^1A_1 \rightarrow 2^1A_2$ ($\pi \rightarrow 3p_z$)	6.22	0.00	0.00	0.00
$1^1A_1 \rightarrow 2^1B_1$ ($\pi \rightarrow 3p_y$)	6.33	0.030	−13.37	−13.58
$1^1A_1 \rightarrow 3^1A_2$ ($\pi \rightarrow$ 3d)	6.76	0.00	0.00	0.00
$1^1A_1 \rightarrow 2^1B_1$ ($\pi \rightarrow$ 3d)	6.88	0.0018	1.77	1.70
$1^1A_1 \rightarrow 2^1B_2$ ($\pi \rightarrow 3p_x$)	6.90	0.0051	−6.61	−6.31
***N*-Methylpyrrole**				
$1^1A' \rightarrow 1A''$ ($\pi \rightarrow$ 3s)	5.04	4.53×10^{-4}	0.009	0.000
$1^1A' \rightarrow 1A''$ ($\pi \rightarrow \pi^*$)	5.59	0.14	10.84	10.42
$1^1A' \rightarrow 1A''$ ($\pi \rightarrow$ 3s/3p$_z$)	5.72	0.013	1.57	1.61
$1^1A' \rightarrow 1A'$ ($\pi \rightarrow$ 3s)	5.72	0.010	2.65	2.14
$1^1A' \rightarrow 1A'$ ($\pi \rightarrow \pi^*$)	5.85	0.013	−16.49	−16.75
$1^1A' \rightarrow 1A'$ ($\pi \rightarrow 3p_y$)	5.94	0.021	−15.87	−15.93
$1^1A' \rightarrow 1A'$ ($\pi \rightarrow$ 3s/3p$_z$)	6.39	0.0056	−1.34	−1.56
$1^1A' \rightarrow 1A''$ ($\pi \rightarrow$ 3d)	6.44	0.0048	5.07	5.04
$1^1A' \rightarrow 1A'$ ($\pi \rightarrow$ 3d)	6.52	0.028	−22.36	−22.99
$1^1A' \rightarrow 1A''$ ($\pi \rightarrow$ 3d)	6.55	0.0011	5.99	5.97
$1^1A' \rightarrow 1A''$ ($\pi \rightarrow 3p_y$)	6.61	2.52×10^{-5}	0.02	0.04
$1^1A' \rightarrow 1A''$ ($\pi \rightarrow 3p_x$)	6.77	0.0063	25.27	25.80
$1^1A' \rightarrow 1A'$ ($\pi \rightarrow \pi^*$)	6.85	0.24	−57.80	−61.19
2,5-Dimethylpyrrole				
$1^1A' \rightarrow 1A''$ ($\pi \rightarrow$ 3s)	4.60	1.17×10^{-4}	0.044	0.034
$1^1A' \rightarrow 1A'$ ($\pi \rightarrow 3p_y$)	5.09	9.39×10^{-4}	1.72	1.23
$1^1A' \rightarrow 1A''$ ($\pi \rightarrow \pi^*$/3s/3p$_z$)	5.46	0.13	−9.65	−9.34
$1^1A' \rightarrow 1A''$ ($\pi \rightarrow$ 3s/3p$_z$)	5.66	0.052	−10.18	−10.72
$1^1A' \rightarrow 1A'$ ($\pi \rightarrow$ 3s/π^*)	5.75	5.24×10^{-4}	−0.99	−1.00
$1^1A' \rightarrow 1A''$ ($\pi \rightarrow$ 3s/3p$_z$)	5.76	0.020	−14.77	−15.09
$1^1A' \rightarrow 1A'$ ($\pi \rightarrow \pi^*$/3s)	5.77	0.0069	33.15	33.17
$1^1A' \rightarrow 1A'$ ($\pi \rightarrow$ 3d)	6.24	0.0056	7.93	7.75
$1^1A' \rightarrow 1A''$ ($\pi \rightarrow 3p_y$)	6.24	8.29×10^{-4}	4.19	4.20
$1^1A' \rightarrow 1A''$ ($\pi \rightarrow 3p_x$)	6.25	0.031	−8.24	−8.63
$1^1A' \rightarrow 1A''$ ($\pi \rightarrow$ 3d)	6.42	0.077	−12.70	−14.39
$1^1A' \rightarrow 1A'$ ($\pi \rightarrow \pi^*$)	6.48	0.11	5.96	4.21
$1^1A' \rightarrow 1A''$	6.56	6.08×10^{-4}	−1.40	−1.37
$1^1A' \rightarrow 1A'$	6.73	0.024	5.51	5.61
$1^1A' \rightarrow 1A'$ ($\pi \rightarrow$ p$_z$/s)	6.79	0.012	−9.36	−9.39
$1^1A' \rightarrow 1A'$ ($\pi \rightarrow$ p$_z$/s)	6.89	0.0077	3.64	3.45
$1^1A' \rightarrow 1A''$	6.93	0.012	−10.86	−11.71

[a] Energies in eV.

other Rydberg transitions. The transition energies decrease in magnitude going from pyrrole to *N*-methylpyrrole to 2,5-dimethylpyrrole so that further Rydberg states and an additional $\pi \rightarrow \pi^*$ valence transition are predicted to be found below 7 eV in the spectra of *N*-methylpyrrole and 2,5-dimethylpyrrole. The low-energy $\pi \rightarrow \pi^*$ transitions of these molecules are less degenerate than was the case for pyrrole. The results for 2,5-dimethylpyrrole are complicated somewhat by the greater number of states found below 7 eV and significant $\pi \rightarrow \pi^*$ and valence mixing.

The calculated MCD $\mathscr{B}$ terms of pyrrole, *N*-methylpyrrole, and 2,5-dimethylpyrrole are also listed in Table 9, and the simulated MCD spectra obtained from these parameters are compared with experimental results and are presented in Figure 4a−c.

The most striking result from the simulated spectra is that they reproduce the qualitative changes observed when going from pyrrole to *N*-methylpyrrole to 2,5-dimethylpyrrole.

For pyrrole, the presence of two nearly degenerate $\pi \rightarrow \pi^*$ transitions suggests that a pseudo-$\mathscr{A}$ term feature would be observed and the transitions to these two states have large oppositely signed $\mathscr{B}$ terms that are consistent with this observation. However, the $\pi \rightarrow 3p_y$ Rydberg transition that is also nearby in energy has a non-negligible negative $\mathscr{B}$ term that is large enough to completely cancel the positive MCD of the $\pi \rightarrow \pi^*$ ($1^1A_1 \rightarrow 1^1B_2$) transition. Although the *B* term of the Rydberg transition is rather smaller than those of the $\pi \rightarrow \pi^*$ transitions, it must be recalled that the positive and negative MCDs of the latter two transitions largely cancel, allowing the smaller MCD of the Rydberg transition to be influential.

As would be expected, the MCD of the two $\pi \rightarrow \pi^*$ transitions arises mostly from mixing among themselves. The largest contribution to the $\mathscr{B}$ term of the $\pi \rightarrow 3p_y$ transition is caused by mixing with the more intense of the two $\pi \rightarrow \pi^*$ states ($1^1A_1 \rightarrow 1^1B_2$).

The important contributions to the MCD spectrum of *N*-methylpyrrole are similar to those of pyrrole. The lowest-energy $\pi \rightarrow \pi^*$ transition provides positive MCD, while the second $\pi \rightarrow \pi^*$ and the $\pi \rightarrow 3p_y$ have significant negative $\mathscr{B}$ terms. The difference in energy between the two $\pi \rightarrow \pi^*$ transitions is greater and the $\pi \rightarrow 3p_y$ transition is further away in energy from the lowest $\pi \rightarrow \pi^*$ transition than was the case for pyrrole. The cancellation of the positive MCD of the $\pi \rightarrow \pi^*$ transition is now incomplete, leading to the positive band observed at around 5.3 eV in Figure 4b. The positive band in the simulated spectrum is somewhat weaker than is observed experimentally, suggesting that the calculated positive $\mathscr{B}$ term is too small, the negative $\mathscr{B}$ terms are too large, or the separation between the $\pi \rightarrow \pi^*$ transitions is underestimated.

The qualitative shape of the simulated MCD spectrum of 2,5-dimethylpyrrole is correct. The computed spectrum has negative MCD at the lowest energies, followed by positive MCD at higher energies and negative MCD at still higher energies, similarly to the experimental spectrum. The band minima and maximum of the simulated spectrum are shifted to higher energies, and the low-energy minimum is somewhat more intense compared with experimental results. From Table 9, it is apparent that several states contribute to the MCD observed in this region. It is therefore very difficult to discern why the simulated spectrum is in error as a number of possible reasons can be proposed, such as overestimation of the negative $\mathscr{B}$ term of the lower-energy transitions, errors in the calculated transition energies, and so on.

In the cases of pyrrole and *N*-methylpyrrole, the majority of the observed MCD was caused by the mixing of three states, the two lowest $\pi \rightarrow \pi^*$ states and the $\pi \rightarrow 3p_y$ state. The two lowest $\pi \rightarrow \pi^*$ states still make significant contributions to the MCD of 2,5-dimethylpyrrole, but the $\pi \rightarrow 3p_y$ transition only has a small $\mathscr{B}$ term. In contrast to the other two nitrogen-containing heterocycles discussed here,

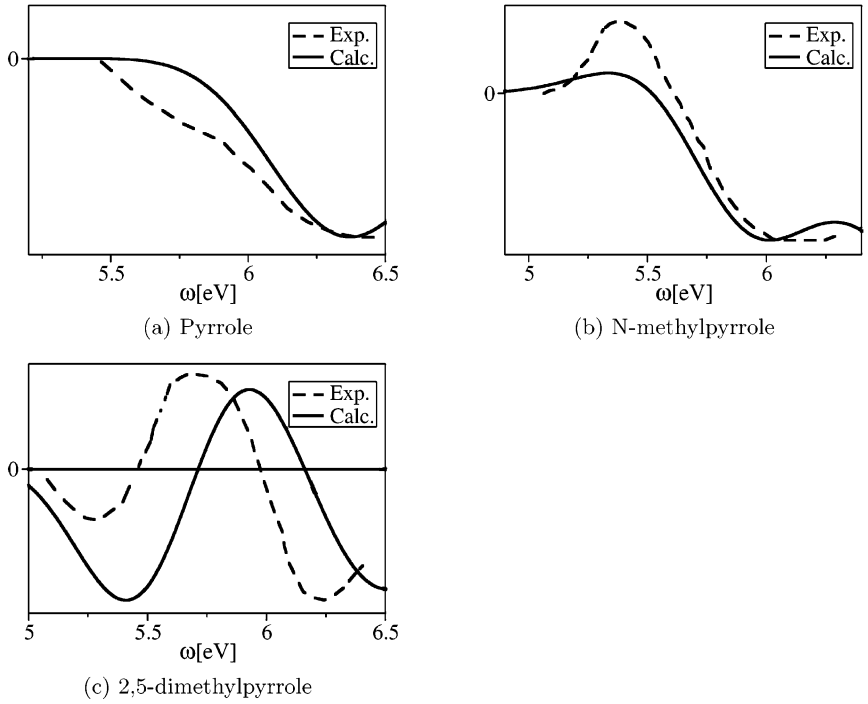

Figure 4. Experimental and simulated MCD spectra of pyrrole, *N*-methylpyrrole, and 2,5-dimethylpyrrole.

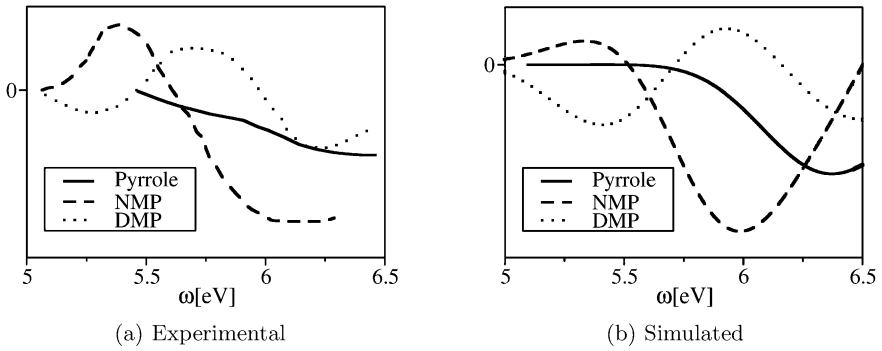

Figure 5. Experimental and simulated MCD spectra pyrrole, *N*-methylpyrrole, and 2,5-dimethylpyrrole.

the lower of the two $\pi \rightarrow \pi^*$ transitions has a negative $\mathscr{B}$ term and the higher has a positive $\mathscr{B}$ term. Several other transitions in the same region make significant contributions to the MCD, but the reversal in sign of the $\mathscr{B}$ terms of the two $\pi \rightarrow \pi^*$ transitions is chiefly responsible for the qualitative change in the spectrum when going from *N*-methylpyrrole to 2,5-dimethylpyrrole. In terms of eq 6, the changes in sign of the $\pi \rightarrow \pi^*$ $\mathscr{B}$ terms arise because the integral $\langle J|\mathbf{L}|K\rangle$ changes sign. Thus, mixing of the lower-energy $\pi \rightarrow \pi^*$ state into the higher-energy $\pi \rightarrow \pi^*$ state makes a positive contribution to the $\mathscr{B}$ term of the higher state rather than a negative contribution.

The experimental MCD spectra of pyrrole, *N*-methylpyrrole, and 2,5-dimethylpyrrole are placed alongside each other in Figure 5a, and the calculated spectra of the same three molecules are compared in Figure 5b. Much like the furan and homologues case, the calculated spectra do a reasonable job of reproducing the relative intensities of the three spectra.

4. Conclusion

In this paper, an approach for calculating the $\mathscr{B}$ terms of MCD spectroscopy was described. The method makes use of the standard formula for the $\mathscr{B}$ term[2] and takes all of the necessary integrals and energies from a TDDFT calculation. As such, it should be possible to calculate the $\mathscr{B}$ terms of any molecule for which a TDDFT calculation can be performed. Once the TDDFT calculation has been performed, the effort required to calculate the $\mathscr{B}$ term scales as the square of the number of transitions obtained and linearly with the size of the transition vectors. As such, $\mathscr{B}$-term calculations can become quite computationally expensive, especially if large numbers of states are included. Current work aimed at improving the scaling to linear in the number of transitions is in progress. The test calculations described here demonstrate that the SOS expansion of the $\mathscr{B}$ term often converges quite quickly, allowing small TDDFT calculations to be performed. MCD spectra that are dominated by pseudo-$\mathscr{A}$ terms arising because of near degeneracies, like that of thiophene, are expected to be described particularly well with this approach as they require small SOS expansions to give a good description of the spectrum.

It must be recalled that the present approach relies heavily on a reasonable starting point from a TDDFT calculation. If the TDDFT calculation is poor because of an inappropriate

choice of functional or a limited basis set, then the chances of obtaining a reasonable $\mathscr{B}$ term are not good.

The $\mathscr{B}$ terms of nine molecules, ethene, propene, furan and three of its homologues, and pyrrole and two of its derivatives, were calculated. Like other calculations, the present work was unable to find the source of the third observed MCD band in the spectra of ethene and propene. On the other hand, almost all of the features of the MCD spectra of the aromatic heterocycles could be reproduced, including the qualitative form of the spectra, many of the quantitative aspects of the spectra, and the trends in MCD intensity between spectra. These closely related molecules show quite a bit of variation in their MCD spectra, all of which could be reproduced and explained.

With the completion of this work, we have now demonstrated how to calculate all contributions to the MCD spectrum assuming that spin−orbit coupling is small and that the MCD varies linearly with the magnetic field. This covers a large number of published spectra, but many modern applications of MCD spectroscopy focus on applications where nonlinearity and spin−orbit coupling cannot be neglected. In a forthcoming publication, we shall describe our attempts to introduce spin−orbit coupling into our MCD formulation.

Acknowledgment. T.Z. would like to thank the Canadian government for a Canada research chair in theoretical inorganic chemistry. J.A. acknowledges financial support from the CAREER program of the National Science Foundation (CHE 0447321).

References

(1) Stephens, P. J. *Ann. Rev. Phys. Chem.* **1974**, *25*, 201−232.

(2) Piepho, S. B.; Schatz, P. N. *Group Theory in Spectroscopy With Applications to Magnetic Circular Dichroism*; John Wiley and Sons: New York, 1983.

(3) Mason, W. R. *Inorg. Chem.* **1989**, *28*, 2487−2489.

(4) Upton, A. H. P.; Williamson, B. E. *J. Phys. Chem.* **1994**, *98*, 71−76.

(5) Seth, M.; Ziegler, T.; Banerjee, A.; Autschbach, J.; van Gisbergen, S. J. A.; Baerends, E. J. *J. Chem. Phys.* **2004**, *120*, 10942−10954.

(6) Seth, M.; Autschbach, J.; Ziegler, T. *J. Chem. Phys.* **2005**, *122*, 094112-1−094112-7.

(7) Seth, M.; Ziegler, T. *J. Chem. Phys.* **2006**, *124*, 144105-1−144105-12.

(8) Michl, J. *Tetrahedron* **1984**, *40*, 3845−3934.

(9) Coriani, S.; Jorgensen, P.; Rizzo, A.; Ruud, K.; Olsen, J. *Chem. Phys. Lett.* **1999**, *300*, 61−68.

(10) Honda, Y.; Hada, M.; Ehara, M.; Nakatsuji, H.; Downing, J.; Michl, J. *Chem. Phys. Lett.* **2002**, *355*, 219−225.

(11) Honda, Y.; Hada, M.; Ehara, M.; Nakatsuji, H.; Downing, J.; Michl, J. *J. Chem. Phys.* **2005**, *123*, 164113-1−164113-9.

(12) Casida, M. E. Time-Dependent Density Functional Response Theory for Molecules. In *Recent Advances in Density Functional Theory, Part 1*; Chang, D. P., Ed.; World Scientific: Singapore, 1995; pp 155−192.

(13) Autschbach, J.; Ziegler, T. *J. Chem. Phys.* **2002**, *116*, 891−896.

(14) Furche, F.; Ahlrichs, R. *J. Chem. Phys.* **2002**, 7433−7447.

(15) te Velde, G.; Bickelhaupt, F. M.; Baerends, E. J.; Fonseca Guerra, C.; van Gisbergen, S. J. A.; Snijders, J. G.; Ziegler, T. *J. Comput. Chem.* **2001**, *22*, 931−967.

(16) Baerends, E. J.; Ellis, D. E.; Ros, P. *Chem. Phys.* **1973**, *2*, 41−51.

(17) Versluis, L.; Ziegler, T. *J. Chem. Phys.* **1988**, *88*, 322−328.

(18) te Velde, G.; Baerends, E. J. *Phys. Rev. B: Condens. Matter Mater. Phys.* **1991**, *44*, 7888−7903.

(19) Fonseca Guerra, C.; Snijders, J. G.; te Velde, G.; Baerends, E. J. *Theor. Chim. Acta* **1998**, *99*, 391−403.

(20) Becke, A. D. *Phys. Rev. A: At., Mol., Opt. Phys.* **1988**, *38*, 3098−3100.

(21) Perdew, J. P. *Phys. Rev. B: Condens. Matter Mater. Phys.* **1986**, *33*, 8822−8824.

(22) Perdew, J. P. *Phys. Rev. B: Condens. Matter Mater. Phys.* **1986**, *34*, 7406.

(23) van Lenthe, E.; Baerends, E. J.; Snijders, J. G. *J. Chem. Phys.* **1993**, *99*, 4597−4610.

(24) van Lenthe, E.; Baerends, E. J.; Snijders, J. G. *J. Chem. Phys.* **1994**, *101*, 9783−9792.

(25) van Lenthe, E.; Ehlers, Æ.; Baerends, E. J. *J. Chem. Phys.* **1999**, *110*, 8943−8953.

(26) Gritsenko, O. V.; Schipper, P. R. T.; Baerends, E. J. *Chem. Phys. Lett.* **1999**, *302*, 199−207.

(27) Schipper, P. R. T.; Gritsenko, O. V.; van Gisbergen, S. J. A.; Baerends, E. J. *J. Chem. Phys.* **2000**, *112*, 1344−1352.

(28) Brith-Lindner, M.; Allen, S. D. *Chem. Phys. Lett.* **1977**, *47*, 32−35.

(29) Syder, P. A.; Atanasova, S.; Hansen, R. W. C. *J. Phys. Chem. A* **2004**, *108*, 4194−4201.

(30) Merer, A. J.; Mulliken, R. S. *Chem. Rev.* **1969**, *69*, 639−656.

(31) Petrongolo, C.; Buenker, R. J.; Peyerimhoff, S. D. *J. Chem. Phys.* **1982**, *76*, 3655−3667.

(32) Sension, R. J.; Hudson, B. S. *J. Chem. Phys.* **1989**, *90*, 1377−1389.

(33) Serrano-Andrés, L.; Mechán, M.; Nebot-Gil, I.; Lindh, R.; Roos, B. O. *J. Chem. Phys.* **1993**, *98*, 3151−3162.

(34) Ryu, J.; Hudson, B. S. *Chem. Phys. Lett.* **1995**, *245*, 448.

(35) Baeck, K. K.; Martinez, T. J. *Chem. Phys. Lett.* **2003**, *375*, 299−308.

(36) Barbatti, M.; Paier, J.; Lischka, H. *J. Chem. Phys.* **2004**, *121*, 11614−11624.

(37) Hazra, A.; Chang, H. H.; Nooijen, M. *J. Chem. Phys.* **2004**, *121*, 2125−2136.

(38) Walker, I. C.; Abuain, T. M.; Palmer, M. H.; Beveridge, A. J. *Chem. Phys.* **1986**, *109*, 269−275.

(39) Håkansson, R.; Nordén, B.; Thulstrup, E. W. *Chem. Phys. Lett.* **1977**, *50*, 305−308.

(40) Nordén, B.; Håkansson, R.; Pedersen, P. B.; Thulstrup, E. W. *Chem. Phys.* **1978**, *33*, 355−366.

(41) Hieringer, W.; van Gisbergen, S. J. A.; Baerends, E. J. *J. Phys. Chem. A* **2002**, *106*, 10380−10390.

(42) Pickett, L. W. *J. Chem. Phys.* **1940**, *8*, 293−297.

(43) Pickett, N. J. H.; Liu, T. C. *J. Am. Chem. Soc.* **1951**, *73*, 4865−4869.

(44) Watanabe, K.; Nakyama, T. *J. Chem. Phys.* **1958**, *29*, 48−51.

(45) Sanche, L. *J. Chem. Phys.* **1979**, *71*, 4860−4882.

(46) Cooper, C. D.; Williamson, A. D.; Miller, J. C.; Compton, R. N. *J. Chem. Phys.* **1980**, *73*, 1527−1537.

(47) Roebber, J. L.; Gerrity, D. P.; Hemley, R.; Vaida, V. *Chem. Phys. Lett.* **1980**, *75*, 104−106.

(48) Serrano-Andrés, L.; Mechán, M.; Nebot-Gil, I.; Roos, B. O.; Fülscher, M. *J. Am. Chem. Soc.* **1993**, *115*, 6184−6197.

(49) Palmer, M. H.; Walker, I. C.; Ballard, C. C.; Guest, M. F. *Chem. Phys.* **1995**, *192*, 111.

(50) Trofimov, A. B.; Schirmer, J. *Chem. Phys.* **1997**, *224*, 175.

(51) Christiansen, O.; Jorgensen, P. *J. Am. Chem. Soc.* **1998**, *120*, 3423−3430.

(52) Burcl, R.; Amos, R. D.; Handy, N. C. *Chem. Phys. Lett.* **2002**, *355*, 8−18.

(53) Hazra, A.; Nooijen, M. *Int. J. Quantum Chem.* **2003**, *95*, 643−657.

(54) Gromov, E. V.; Trofimov, A. B.; Vitkovskaya, N. M.; Schirmer, J.; Köppel, H. *J. Chem. Phys.* **2003**, *119*, 737−751.

(55) Christiansen, O.; Gauss, J.; Stanton, J. F.; Jorgensen, P. *J. Chem. Phys.* **1999**, *111*, 525−537.

(56) Roos, B. O.; Malmqvist, P.-Å; Molina, V.; Serrano-Andrés, L.; Merchán, M. *J. Chem. Phys.* **2002**, *116*, 7526−7536.

(57) Palmer, M. H.; Wilson, P. J. *Mol. Phys.* **2003**, *101*, 2391−2408.

(58) Pastore, M.; Angeli, C.; Cimiraglia, R. *Chem. Phys. Lett.* **2006**, *422*, 522−528.

CT600283T